Evaluation of the Common Mode and the Differential Mode Components from Conducted Emission Measurements

Michele Perotti, *Member, IEEE,* and Franco Fiori, *Member, IEEE*

***Abstract*—The design of the power supply EMI filter needed to mitigate the conducted emission of electronic modules can be performed best if the magnitude of the common mode and that of the differential mode interference are known. In common test setups the two terms can be obtained from the signals measured at the line impedance stabilization networks (LISNs) output ports using differential- and common-mode rejection networks or through the post-processing of the output signals in the time domain. Both these approaches rely on the perfect matching of the LISNs internal filters, which is not realistic. In practice, the LISNs mismatch allow the differential mode (DM) to be measured as common mode (CM) and vice versa. In this work the influence of the LISNs mismatch on the separation of CM and DM is investigated and a fast and accurate method to do that is proposed.**

***Index Terms*—Line Impedance Stabilization Network (LISN), conducted emission measurement, calibration, differential mode rejection, modal conversion,**

I. Introduction

The compliance of electronic equipments or modules to electromagnetic compatibility (EMC) international standards, such as CISPR or ISO [1]–[3], or to design specifications, can be achieved only if the power spectral density of the electromagnetic interference (EMI) they generate is below the limits suggested by the standard itself or defined by the manufacturer. Usually, such documents provide a detailed description of the test setup to be used. About those prescribed for conducted emission measurements, they require the use of one or two LISNs depending on whether the power supply of the equipment under test (EUT) is referred to the metal chassis locally or remotely with power cables. In the latter case, i.e., with two LISNs, the conducted emission measured at the two LISNs output ports can be used to evaluate the common mode (CM) and the differential mode (DM) emission spectra, which in turn can be used for the design of the EUT's EMI filter [4]. Indeed, an error in the evaluation of the emission components could result in oversized or undersized EMI filters that may affect either the EUT physical dimensions or the emission levels [5].

For that reason, a variety of hardware and software separation techniques have been proposed over time. The hardware separation techniques require the connection of a network to the two LISNs outputs, which rejects the CM or the DM interference. These networks can be used to measure only one mode [6], or to measure both emission modes, separately [7]–[10]. Other techniques have been developed, based on a software approach, as in [11]. In that work the conducted emission at the LISNs' output ports is measured directly in the time domain, then processed in order to obtain the CM and the DM components. An alternative to the time domain measurement at the LISNs' output ports consists in measuring the CM and the DM currents delivered by the EUT with a current probe clamped to the EUT power supply cables and connected to an EMI receiver. By doing so, the currents flowing in the cables are measured but being the relationship with the voltages measured at the LISN ouputs not straightforward, their spectra cannot be compared with the emission limit suggested by the standard, which are defined in terms of voltages at the LISNs output ports [12]. All the previously presented approaches that allow one to separate the CM and the DM interference are based on the assumption that the two LISNs are perfectly matched. However, this is not possible in practice even if the two LISNs are calibrated. Indeed, the standards define a tolerance band for the LISN impedance [1] so that, two LISNs, which are compliant with the standard and a part of the same test setup, can show differences in their respective impedance. This turns out to be the cause of conversion of DM into CM and vice versa. In literature, the modal conversion has been analyzed in other fields, such as differential transmission lines [13], [14] or EMC test procedures [15]. Moreover, the mismatch of the parasitic elements of active or passive components was already investigated in previous works to evaluate the modal conversion of the EMI in DC-DC converters [16] or to compensate the EMI filter imbalance [17]. Ultimately, none of these works address the problem of separating the CM from the DM in a real conducted emission test setup [1].

Actually, the LISNs mismatch issue was firstly highlighted in [12], where a method based on the use of current probes was proposed. That work considers the modal conversion, due to the differences between the two LISNs' impedances, only as a loss of performance in separating the two modes, without proposing a possible solution to address the issue.

The present paper analyzes the sources of modal conversion and proposes a method to separate the CM and the DM, effectively. This is based on the experimental characterization of the CISPR 25 test setup in terms of scattering parameters and on

M. Perotti and F. Fiori are with the Department of Electronics and Telecommunications, Politecnico di Torino, Turin, 10129 Italy, e-mail: franco.fiori@polito.it.

This work was partially supported by the Power Electronics Innovation Center (PEIC) of the Politecnico di Torino.

Manuscript received XX XX, 2021; revised XX XX, 202X.

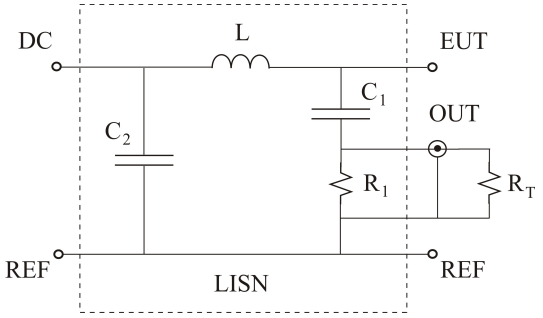

Fig. 1. LISN schematic view according to CISPR 25.

the measurement in the time domain of the conducted emission at the LISNs output ports. Indeed, the modal conversion caused by the LISNs mismatch can be removed completely.

The paper is organized as follows: Section II introduces the test setup prescribed by CISPR 25 to measure the conducted emission of electronic modules. Section III discusses the main causes of modal conversion in such a test setup. A method to obtain the CM and the DM components from the voltages measured at the LISNs output ports is proposed in Section IV and V. The validation of the proposed approach is presented in Section VI along with a use case on the conducted emission generated by a power inverter. Concluding remarks are drawn in Section VII.

II. Conducted Emission Measurement

Electromagnetic emissions are regulated by international standards, such as CISPR 25 [1] for automotive equipments. This standard has been taken as a reference for the following analyses; however, the same conclusions can be drawn using, for example, the testing guidelines for household appliances [2]. CISPR 25 defines the measurement setup for different apparatus and provides the emission limits for both radiated and conducted emission. Focusing on the conducted emission, it requires the connection of one or two LISNs between the power supply and the EUT in order to define a standard power supply impedance over the frequency range of interest. The LISN circuit as it can be found in the standard is shown in Fig. 1. Both the LISNs' REF terminals should be connected to a copper reference plane. The EUT is connected to the LISNs and it is isolated from the reference plane by a low permittivity support, whose thickness is 50±5 mm. The LISN's output port has to be loaded with $R_{\mathrm{T}} = 50\ \Omega$ termination, which can be a real one or the input impedance of the measuring instrument. The conducted emission measurements are performed in the frequency bands 0.15 - 30 MHz and 30 - 108 MHz.

Furthermore, CISPR 25 prescribes different test setups depending on the EUT features and on its ground connection. In particular, for remotely grounded equipment, i.e., for ground connection cables longer than 200 mm, and for alternators and generators, two LISNs to perform the conducted EMI measurements, one connected to the positive power supply terminal and the other connected to the negative one, are required. This test setup is shown in Fig. 2. The emission is measured with an EMI receiver connected to one of the

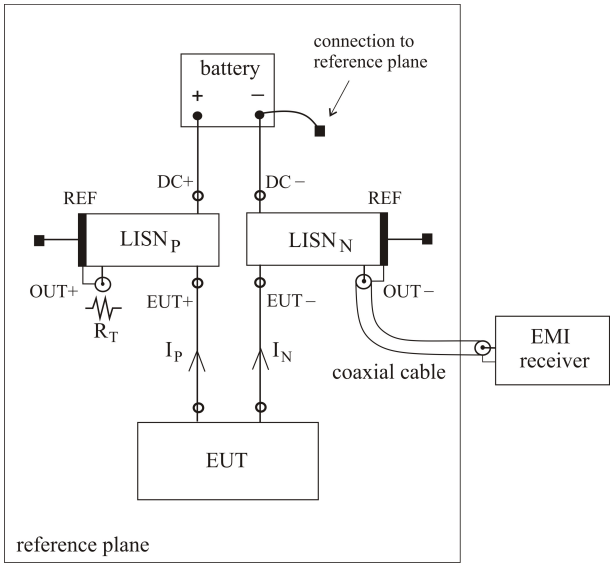

Fig. 2. Test setup for remotely grounded EUT and for alternators and generators.

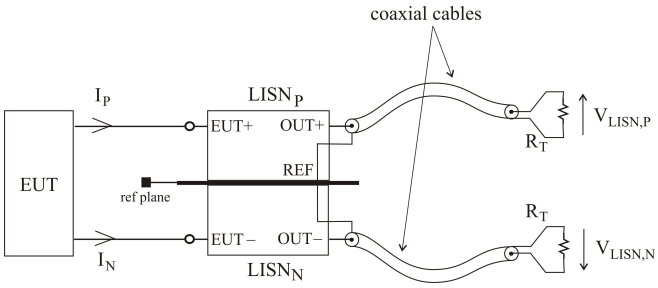

Fig. 3. Schematic view of the test setup used to define the voltages and the currents of interest.

two LISNs output ports, while having the other one loaded by a 50 Ω termination.

Such a test method can be used for evaluating the compliance of the EUT to the emission limit or to obtain the CM and the DM components of the conducted emission, which are needed for the design of the power supply EMI filter. Usually, they are evaluated as

$$V_{\mathrm{CM}}^{(m)} = \frac{1}{2}\left(V_{\mathrm{LISN,p}} + V_{\mathrm{LISN,n}}\right), \tag{1}$$

$$V_{\mathrm{DM}}^{(m)} = V_{\mathrm{LISN,p}} - V_{\mathrm{LISN,n}}, \tag{2}$$

where $V_{\mathrm{CM}}^{(m)}$ and $V_{\mathrm{DM}}^{(m)}$ are the CM and the DM voltages calculated from those measured at the LISNs ports, i.e., $V_{\mathrm{LISN,p}}$ and $V_{\mathrm{LISN,n}}$, the voltages across the termination resistances. In the following section, the evaluation of the CM and DM from the voltages measured at the LISNs output ports is introduced.

III. Evaluation of the CM and the DM conducted emission from measurements

The voltages measured at the LISNs output ports are due to the high frequency currents flowing through the EUT power supply cables, namely I_{P} and I_{N} in Fig. 2. These can be used

to define the CM and the DM currents flowing in the power supply cables as

$$I_{\mathrm{CM}} \triangleq \left(\frac{I_{\mathrm{P}} + I_{\mathrm{N}}}{2}\right), \tag{3}$$

$$I_{\mathrm{DM}} \triangleq (I_{\mathrm{P}} - I_{\mathrm{N}}). \tag{4}$$

Therefore I_{P} and I_{N} can be written as

$$I_{\mathrm{P}} = I_{\mathrm{CM}} + \frac{I_{\mathrm{DM}}}{2}, \tag{5}$$

$$I_{\mathrm{N}} = I_{\mathrm{CM}} - \frac{I_{\mathrm{DM}}}{2}. \tag{6}$$

Since the two LISNs comprise of linear passive components, the voltages at the output ports can be expressed as

$$V_{\mathrm{CM}}^{(m)} = V_{\mathrm{CM}}^{\mathrm{DM}} + V_{\mathrm{CM}}^{\mathrm{CM}}, \tag{7}$$

i.e., the CM voltage due to the DM excitation ($V_{\mathrm{CM}}^{\mathrm{DM}}$) plus that due CM one ($V_{\mathrm{CM}}^{\mathrm{DM}}$). Similarly, for the DM voltage, it results

$$V_{\mathrm{DM}}^{(m)} = V_{\mathrm{DM}}^{\mathrm{DM}} + V_{\mathrm{DM}}^{\mathrm{CM}}. \tag{8}$$

These can be expressed as a function of the CM and the DM current as

$$\begin{pmatrix} V_{\mathrm{CM}}^{(m)} \\ V_{\mathrm{DM}}^{(m)} \end{pmatrix} = \mathbf{F} \cdot \begin{pmatrix} \frac{I_{\mathrm{DM}}}{2} \\ 2I_{\mathrm{CM}} \end{pmatrix}, \tag{9}$$

where

$$\mathbf{F} = \begin{pmatrix} F_{\mathrm{CM}}^{\mathrm{DM}} & F_{\mathrm{CM}}^{\mathrm{CM}} \\ F_{\mathrm{DM}}^{\mathrm{DM}} & F_{\mathrm{DM}}^{\mathrm{CM}} \end{pmatrix}. \tag{10}$$

The superscripts indicate the source component (CM or DM), the subscripts the output mode. Ideally, if the two LISNs were perfectly matched, the CM voltage $V_{\mathrm{CM}}^{(m)}$ would depend on the CM current only as $V_{\mathrm{CM}}^{(m)} = F_{\mathrm{CM}}^{\mathrm{CM}}(2I_{\mathrm{CM}})$, and the DM voltage would be $V_{\mathrm{DM}}^{(m)} = F_{\mathrm{DM}}^{\mathrm{DM}}(I_{\mathrm{DM}}/2)$. Actually, a mismatch between the two LISNs always exists, therefore the CM voltage ($V_{\mathrm{CM}}^{(m)}$) obtained by (1) is affected by the DM current, and similarly the DM voltage ($V_{\mathrm{DM}}^{(m)}$) is affected by the CM current. The different causes of the LISN mismatch are deepened in what follows.

A. LISN tolerance contribution

The first cause of modal conversion we consider is that due to the mismatch of the LISNs' input impedances. This is due to the fabrication tolerance of the components the LISNs are made of, their parasitic elements and those due to the LISNs internal layout and packaging. In order to comply with CISPR 25, the input impedance should be within $\pm 20\%$ of the reference values, as tabulated in Annex E [1]. The expression of the input impedance can be derived from the analysis of the circuit shown in Fig. 1 with the DC input shorted to REF. From this analysis it results

$$Z_{\mathrm{LISN}} = \frac{sL(1 + s(R_1 \parallel R_{\mathrm{T}})C_1)}{s^2 LC_1 + s(R_1 \parallel R_{\mathrm{T}})C_1 + 1}, \tag{11}$$

where L, C_1, C_2, R_1 are the circuit parameters, R_{T} is the termination resistance connected to the LISN output port. The magnitude of such an impedance can be evaluated referring to the circuit parameters listed in the standard, i.e., $L = 5\ \mu\mathrm{H}$ $C_1 = 100$ nF, $C_2 = 1\ \mu$F, $R_1 = 1\ \mathrm{k}\Omega$ and $R_{\mathrm{T}} = 50\ \Omega$, obtaining the values shown by continuous line in Fig. 4. The range prescribed by the standard is shown in the same figure by dashed lines. Therefore, the impedance magnitude of two LISNs compliant to CISPR 25 may differ by $\pm 20\%$ causing the modal conversion highlighted in (9).

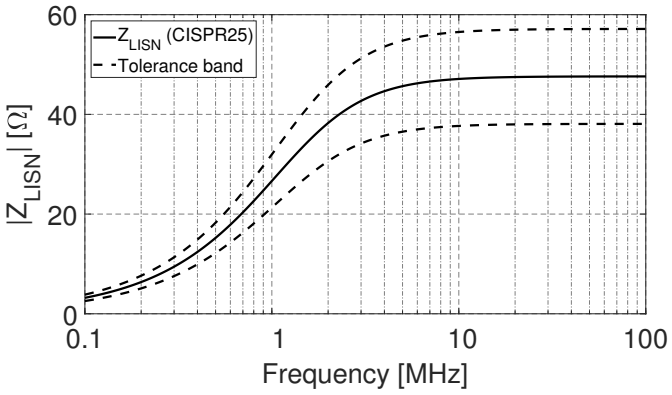

Fig. 4. LISN impedance and tolerance band according to CISPR25.

The mismatch of the LISNs' input impedances is not the sole cause of modal conversion and other contributions should be taken into account, as discussed in the sections below.

B. Interconnection cable mismatch

Besides the mismatch of the LISNs input impedance, another contribution to the modal conversion results from the cables connecting the LISNs output ports to the measuring instrument. Indeed, if the two cables are not the same length, or they show different phase velocity, a phase shift at the input ports of the measuring instrument is experienced. The time delay introduced by two lossless coaxial cables affected by length mismatch can be expressed as

$$\begin{aligned} \tau_{\mathrm{p}} &= \tfrac{l}{v} = \tau, \\ \tau_{\mathrm{n}} &= \tfrac{l+\Delta l}{v} = \tau + \Delta t, \end{aligned} \tag{12}$$

where τ_{p} (τ_{n}) is the delay due to the coaxial cables connecting the $\mathrm{LISN_p}$ ($\mathrm{LISN_n}$) output port to the measuring instrument, v is the cable propagation velocity, l is the cables' nominal length, Δl is the length mismatch. Δt is the delay difference resulting from the length mismatch that may result from the mismatch of the phase velocity as well. Based on that, the modal conversion due to the cables mismatch can be evaluated referring to the schematic view shown in Fig. 5(a). In here, the two cables are assumed to be perfectly matched at the receiver side (R_{T}) and driven by a CM voltage source at the LISNs side (V_{CM}). The modal conversion term due to the cable mismatch, i.e., $V_{\mathrm{DM}}^{\mathrm{CM}}$ can be expressed as

$$\begin{aligned} V_{\mathrm{DM}}^{\mathrm{CM}} &= V_{\mathrm{LISN,p}}^{\mathrm{CM}} - V_{\mathrm{LISN,n}}^{\mathrm{CM}} \\ &= V_{\mathrm{CM}} e^{(-j\omega\tau)} - V_{\mathrm{CM}} e^{(-j\omega(\tau+\Delta t))}, \end{aligned} \tag{13}$$

which magnitude is

$$\left|V_{\mathrm{DM}}^{\mathrm{CM}}\right| = V_{\mathrm{CM}} \sqrt{2\,(1 - \cos(\omega \Delta t))}. \tag{14}$$

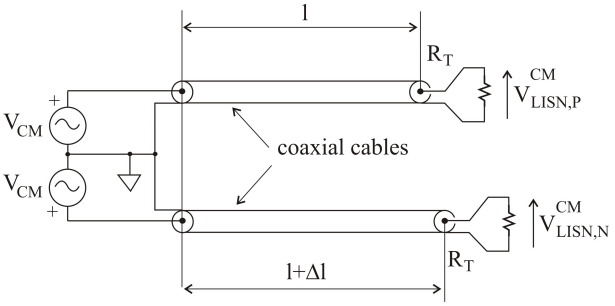

(a) *CM excitation.*

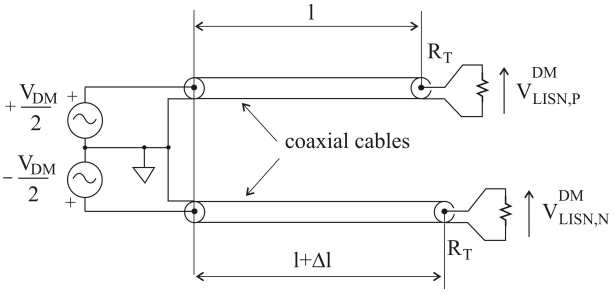

(b) *DM excitation.*

Fig. 5. Interconnection cable mismatch.

Similarly, with the two cables driven at the LISNs side by two ideal DM voltage sources ($V_{\mathrm{DM}}/2$) (see Fig. 5(b)), the CM voltage at the receiver side ($V_{\mathrm{CM}}^{\mathrm{DM}}$) can be written as

$$\begin{aligned} V_{\mathrm{CM}}^{\mathrm{DM}} &= \frac{1}{2}\left(V_{\mathrm{LISN,p}}^{\mathrm{DM}} + V_{\mathrm{LISN,n}}^{\mathrm{DM}}\right) \\ &= \frac{1}{2}\left[\frac{V_{\mathrm{DM}}}{2}e^{(-j\omega\tau)} - \frac{V_{\mathrm{DM}}}{2}e^{(-j\omega(\tau+\Delta t))}\right], \end{aligned} \tag{15}$$

whose magnitude can be expressed as

$$\left|V_{\mathrm{CM}}^{\mathrm{DM}}\right| = V_{\mathrm{DM}}\sqrt{\frac{1-\cos(\omega\Delta t)}{8}}. \tag{16}$$

(14) and (16) may be used to evaluate the modal conversion terms in the worst case. Indeed, at the highest frequency, i.e., $f = 108$ MHz, and assuming the length mismatch $\Delta l = 1$ cm, the DM due to the CM source, i.e., $\left|V_{\mathrm{DM}}^{\mathrm{CM}}\right|$ is about 30 dB below the CM (V_{CM}) and the CM due to the DM sources, i.e., $\left|V_{\mathrm{CM}}^{\mathrm{DM}}\right|$ is about 45 dB below the DM (V_{CM}). Based on the above, and considering that the length mismatch of two equal cables is usually well below 1 cm, it can be concluded that the cable mismatch contributes to the modal conversion negligibly.

C. Influence of the battery impedance

The conversion of the DM (CM) into CM (DM) can be also ascribed to the impedance shown by the dc power supply connected to the LISNs DC+ and DC- terminals (see the battery in Fig. 2), and whether the battery negative terminal is connected to the reference plane or not. Wanting to deepen on that, the circuit shown in Fig. 6 was considered. It comprises of the two LISN equivalent circuits, the battery impedance Z_{PS} and the impedance of the cable connecting the negative terminal to the reference plane Z_{C}. Furthermore, the two

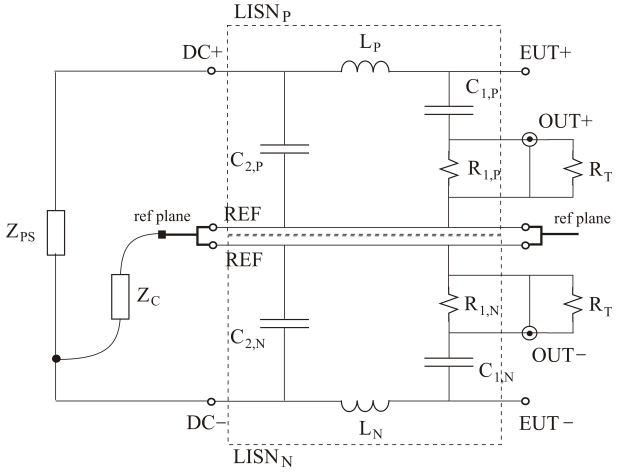

Fig. 6. Equivalent circuit of the two LISNs including the impedance of the dc power supply (Z_{PS}), that of the bonding connecting the battery negative pole to the reference plane (Z_{C}) and the termination resistances (R_{T}) at the output ports.

LISNs were assumed perfectly matched, i.e., $C_{1,\mathrm{P}} = C_{1,\mathrm{N}}$, $C_{2,\mathrm{P}} = C_{2,\mathrm{N}}$, $R_{1,\mathrm{P}} = R_{1,\mathrm{N}}$, $L_{\mathrm{P}} = L_{\mathrm{N}}$. The analysis we performed in this case highlighted that as long as the battery is isolated from the reference plane, i.e., $|Z_{\mathrm{C}}| \to \infty$, its impedance does not cause any modal conversion. On vice versa, with the negative pole connected to the reference plane, the impedance of $C_{2,\mathrm{N}}$ is affected by Z_{C}, since they are in parallel. As a consequence, the circuit loses its symmetry and the modal conversion takes place. Aiming to remove this last contribution along with those mentioned above, the test setup comprising of the two LISNs and the dc power supply was characterized as it is shown below.

IV. Characterization of the Conducted Emission Test Setup

The effective rejection of either the CM or the DM, according to the one that is being measured, can be pursued with the characterization of the test setup. It consists in measuring the scattering matrix of the system, by means of a vector network analyzer (VNA). The system to be measured and its ports are shown in Fig. 7. Port 1 and 2 are the EUT terminals to ground, ports 3 and 4 are the LISNs positive and negative outputs to ground, respectively. The measured scattering matrix can be converted into the impedance matrix, and being

$$\begin{pmatrix} V_1 \\ V_2 \\ V_3 \\ V_4 \end{pmatrix} = \begin{pmatrix} Z_{11} & Z_{12} & Z_{13} & Z_{14} \\ Z_{21} & Z_{22} & Z_{23} & Z_{24} \\ Z_{31} & Z_{32} & Z_{33} & Z_{34} \\ Z_{41} & Z_{42} & Z_{43} & Z_{44} \end{pmatrix} \begin{pmatrix} I_1 \\ I_2 \\ I_3 \\ I_4 \end{pmatrix} \tag{17}$$

where V_i (I_j) is the i-th port voltage (current), Z_{ij} is the generic impedance matrix element, the transfer functions relating the CM and the DM voltages to the EUT CM and DM currents can be derived. Indeed, as far as the DM current

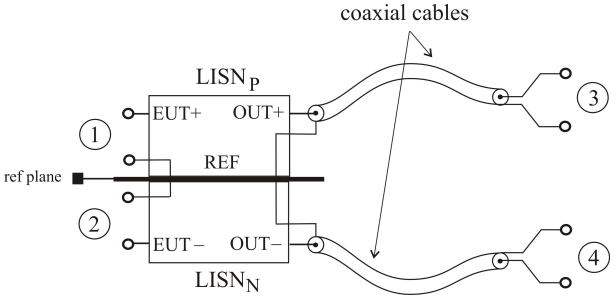

Fig. 7. Definition of the ports considered for the characterization of the test setup. Port numbers are enclosed in circles.

($I_{\rm DM}$) only is concerned and the CM current ($I_{\rm CM}$) is zeroed, it results

$$\begin{cases} I_1^{\rm DM} = -I_2^{\rm DM} \\ I_1^{\rm DM} = \dfrac{I_{\rm DM}}{2} \\ I_3^{\rm DM} = -\dfrac{V_3^{\rm DM}}{R_{\rm T,p}} \\ I_4^{\rm DM} = -\dfrac{V_4^{\rm DM}}{R_{\rm T,n}} \end{cases}, \tag{18}$$

and

$$\begin{pmatrix} 1+\frac{Z_{33}}{R_{\rm T}} & \frac{Z_{34}}{R_{\rm T}} \\ \frac{Z_{43}}{R_{\rm T}} & 1+\frac{Z_{44}}{R_{\rm T}} \end{pmatrix} \cdot \begin{pmatrix} V_3^{\rm DM} \\ V_4^{\rm DM} \end{pmatrix} = \begin{pmatrix} (Z_{31}-Z_{32})\frac{I_{\rm DM}}{2} \\ (Z_{41}-Z_{42})\frac{I_{\rm DM}}{2} \end{pmatrix}. \tag{19}$$

This expression comprises of the third and the fourth rows of (17), which are rewritten to include (18). In particular, $R_{\rm T,p}$, $R_{\rm T,n}$ are the termination resistances loading the positive and negative LISNs' output ports that will be assumed equal to one another from now on, i.e., ($R_{\rm T,p} = R_{\rm T,n} = R_{\rm T}$). Indeed, they represent the input impedance of the same instrument (the oscilloscope) in actual tests. Furthermore, it is worth underlining that the voltages at port 3 and port 4 are those observed at the LISNs output ports, i.e., $V_3^{\rm DM} = V_{\rm LISN,p}^{\rm DM}$ and $V_4^{\rm DM} = V_{\rm LISN,n}^{\rm DM}$ when the inputs are driven by the DM only. Therefore, solving (19) for $V_3^{\rm DM}$, $V_4^{\rm DM}$ and dividing by ($I_{\rm DM}/2$) the CM and DM trans-impedances can be expressed as

$$\begin{aligned} F_{\rm CM}^{\rm DM} &= \left(\frac{V_3^{\rm DM}+V_4^{\rm DM}}{2}\right) / \left(I_{\rm DM}/2\right) = \\ &= \frac{1}{2\Delta}\left[A\left(Z_{31}-Z_{32}\right) - B\left(Z_{42}-Z_{41}\right)\right], \end{aligned} \tag{20}$$

$$\begin{aligned} F_{\rm DM}^{\rm DM} &= \left(V_3^{\rm DM}-V_4^{\rm DM}\right) / \left(I_{\rm DM}/2\right) = \\ &= \frac{1}{\Delta}\left[C\left(Z_{31}-Z_{32}\right) + D\left(Z_{42}-Z_{41}\right)\right], \end{aligned} \tag{21}$$

where

$$A = \left(1+\frac{Z_{44}}{R_{\rm T}}-\frac{Z_{43}}{R_{\rm T}}\right),$$

$$B = \left(1+\frac{Z_{33}}{R_{\rm T}}-\frac{Z_{34}}{R_{\rm T}}\right),$$

$$C = \left(1+\frac{Z_{44}}{R_{\rm T}}+\frac{Z_{43}}{R_{\rm T}}\right),$$

$$D = \left(1+\frac{Z_{33}}{R_{\rm T}}+\frac{Z_{34}}{R_{\rm T}}\right),$$

$$\Delta = \left(1+\frac{Z_{44}}{R_{\rm T}}\right)\left(1+\frac{Z_{33}}{R_{\rm T}}\right) - \left(\frac{Z_{43}}{R_{\rm T}}\right)\left(\frac{Z_{34}}{R_{\rm T}}\right).$$

A similar approach may be used for the CM current. Indeed, having the two LISNs driven by the CM current ($I_{\rm CM}$) only and the DM current ($I_{\rm DM}$) zeroed, it results

$$\begin{cases} I_1^{\rm CM} = I_2^{\rm CM} = I_{\rm CM} \\ I_3^{\rm CM} = -\dfrac{V_3^{\rm CM}}{R_{\rm T}} \\ I_4^{\rm CM} = -\dfrac{V_4^{\rm CM}}{R_{\rm T}} \end{cases}. \tag{22}$$

Therefore, the third and the fourth rows in (17) becomes

$$\begin{pmatrix} 1+\frac{Z_{33}}{R_{\rm T}} & \frac{Z_{34}}{R_{\rm T}} \\ \frac{Z_{43}}{R_{\rm T}} & 1+\frac{Z_{44}}{R_{\rm T}} \end{pmatrix} \cdot \begin{pmatrix} V_3^{\rm CM} \\ V_4^{\rm CM} \end{pmatrix} = \begin{pmatrix} (Z_{31}+Z_{32})I_{\rm CM} \\ (Z_{41}+Z_{42})I_{\rm CM} \end{pmatrix}, \tag{23}$$

and the CM trans-impedances can be expressed as

$$\begin{aligned} F_{\rm DM}^{\rm CM} &= \left(V_3^{\rm CM}-V_4^{\rm CM}\right) / \left(2I_{\rm CM}\right) = \\ &= \frac{1}{2\Delta}\left[C\left(Z_{31}+Z_{32}\right) - D\left(Z_{42}+Z_{41}\right)\right], \end{aligned} \tag{24}$$

$$\begin{aligned} F_{\rm CM}^{\rm CM} &= \left(\frac{V_3^{\rm CM}+V_4^{\rm CM}}{2}\right) / \left(2I_{\rm CM}\right) = \\ &= \frac{1}{4\Delta}\left[A\left(Z_{31}+Z_{32}\right) + B\left(Z_{42}+Z_{41}\right)\right]. \end{aligned} \tag{25}$$

On the basis of (20) and (24), and assuming the cross coupling of the two LISNs negligible, i.e., $Z_{32} = Z_{41} = 0$ and $Z_{43} = Z_{34} = 0$, it can be concluded that the conversion of the DM (CM) into CM (DM) takes place if $Z_{31} \neq Z_{42}$ and $Z_{44} \neq Z_{33}$. Furthermore, it is worth underling that, as far (10) is concerned, the trans-impedances $F_{\rm CM}^{\rm DM}$ and $F_{\rm DM}^{\rm CM}$ are equal to one another.

V. Evaluation of the real CM and DM components

The actual CM and DM components composing the EUT conducted emission can be evaluated using those measured at the positive and negative LISNs output ports. Indeed, from (9), it comes out

$$\begin{pmatrix} \frac{I_{\rm DM}}{2} \\ 2I_{\rm CM} \end{pmatrix} = \mathbf{F^{-1}} \begin{pmatrix} V_{\rm CM}^{(m)} \\ V_{\rm DM}^{(m)} \end{pmatrix}, \tag{26}$$

and the real CM and DM voltages at LISNs outputs not affected by the modal conversion can be expressed as

$$\begin{cases} V_{\rm CM} = F_{\rm CM}^{\rm CM}\left(2I_{\rm CM}\right) \\ V_{\rm DM} = F_{\rm DM}^{\rm DM}\left(\dfrac{I_{\rm DM}}{2}\right) \end{cases}. \tag{27}$$

Therefore, by these expressions one may evaluate the actual CM and DM components of the conducted emission from the voltages measured at the LISNs output ports. To this purpose, it is worth underling that $V_{\rm LISN,p}$ and $V_{\rm LISN,n}$ should be acquired in a synchronous fashion, since the phase relation between them is needed. The error caused by the

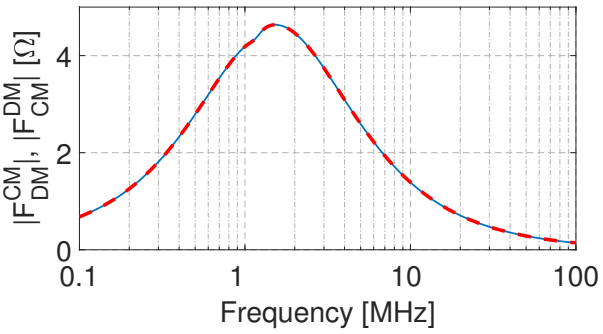

Fig. 8. Modal conversion trans-impedances obtained fron the frequency analysis of the circuit in Fig. 6 for the worst case mismatch of the two LISNs. The continuous line (blue) refers to $F_{\cdot\mathrm{DM}}^{\mathrm{CM}}$, the dashed line (red) to $F_{\mathrm{CM}}^{\mathrm{DM}}$

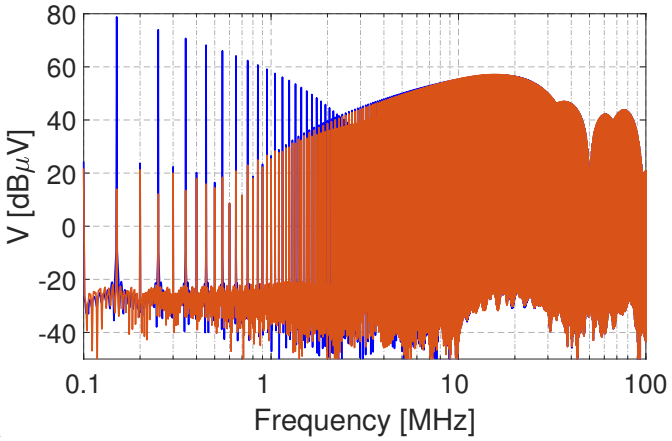

Fig. 9. Simulation results: CM voltage corrupted by the DM (blue line) and CM spectrum after the application of the proposed technique (red line). In the higher frequency range, the two spectra are overlapped.

modal conversion can be evaluated referring to the worst case mismatch allowed by CISPR 25. In particular, as far as the circuit in Fig. 6 is concerned, with parameters $L_{\mathrm{P}} = 5.95\,\mu\mathrm{H}$, $L_{\mathrm{N}} = 4.05\,\mu\mathrm{H}$, $C_{1,\mathrm{P}} = 119\,\mathrm{nF}$, $C_{1,\mathrm{N}} = 81\,\mathrm{nF}$ and $|Z_{\mathrm{PS}}| = |Z_{\mathrm{C}}| = 0$, the modal conversion transfer functions can be obtained from (20) and (24). They are shown in Fig. 8. Furthermore, the time domain analysis of the same circuit driven by two independent sources (not shown in Fig. 6), one generating the CM and the other the DM was carried out. The DM was generated by a triangular shaped current source, at frequency $f = 50\,\mathrm{kHz}$, duty cycle $\delta = 0.5$ and peak amplitude $I_{\mathrm{p}} = 0.2\,\mathrm{A}$. The CM was obtained by two complementary voltage sources generating trapezoidal voltage waveforms at f =50 kHz, duty cycle $\delta = 0.5$, rising/falling time $t_{\mathrm{r}} = t_{\mathrm{f}} = 20\,\mathrm{ns}$ and amplitude $V_{\mathrm{PS}} = 12\,\mathrm{V}$. The voltage waveforms were delayed by 5 ns in order to generate the CM current as in [20]. Each voltage source was coupled to the reference plane by a parasitic capacitance, $C_{\mathrm{p}} = 10\,\mathrm{pF}$. Such analyses provided the output voltages $V_{\mathrm{LISN,p}}$ and $V_{\mathrm{LISN,n}}$, which half sum has the spectrum plotted in Fig. 9 in blue. The same voltages were used to evaluate the actual CM currents with (26), thus obtaining the actual CM voltage with (27). The spectrum of the actual CM voltage is plotted in orange in Fig. 9. On the basis of these results, one can conclude that the removal of the modal conversion terms proposed in this work is needed especially at low frequency, meaning between 150 kHz and 2 MHz.

VI. Method Validation

Wanting to validate the proposed approach, the test bench shown in Fig. 10 was set up. It comprised of the EUT, i.e., an inverter driving a power load, which positive and negative power supply terminals were connected to a dc voltage source through two LISNs [23]. The LISNs' outputs (OUT+ and OUT-) were connected to a 4 GHz, 10 bit resolution oscilloscope [26] by means of 50Ω coaxial cables. Furthermore, an RF current probe [24] was clamped on the cables connecting the power inverter to the LISNs' inputs (EUT+, EUT-). The current probe output was connected to an EMI receiver [25], with the purpose of measuring the CM current directly. A schematic view of the test setup highlighting the power section of the inverter, i.e., the EUT, the parasitic coupling

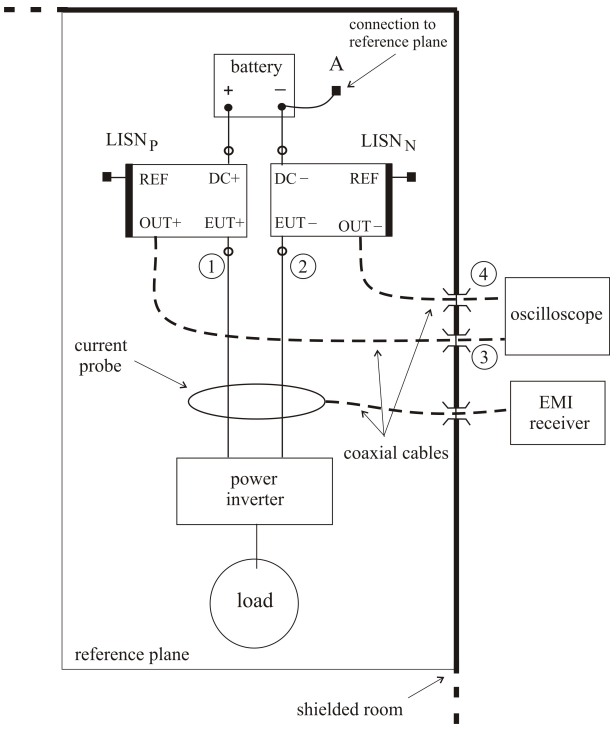

Fig. 10. Schematic view of the test setup used to validate the proposed approach. The voltages at the LISNs' output ports were measured with an oscilloscope, the common mode current with a current probe connected to an EMI receiver.

of its switching nodes with the reference plane (C_{PU}, C_{PV}), the power supply equivalent circuit (V_{PS} and Z_{PS}) and its connection to the reference plane (Z_{C}) is shown in Fig. 11.

Before measuring the conducted emission, the section composed of the LISNs and the dc source (the battery), was characterized in terms of scattering parameters. A four port VNA [21] was connected to the inputs (1 and 2) and to the outputs (3 and 4). Given that the inputs of common LISNs such as those available in our laboratory are not featured to connect coaxial cables, two custom adapters were built and used to connect the RF cable braided shield to the reference

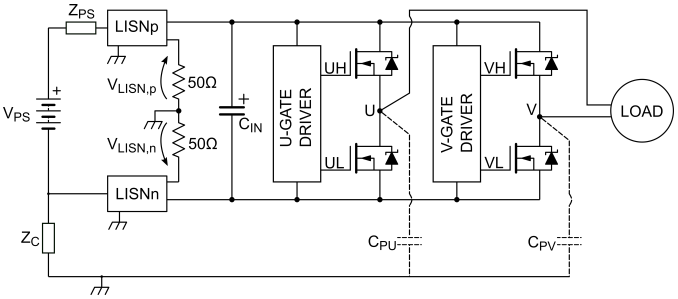

Fig. 11. Schematic description of the power inverter (the EUT) used for the experimental validation of the method.

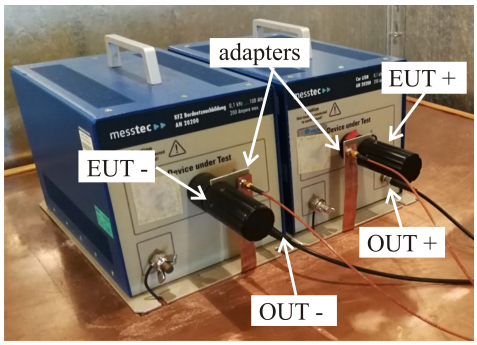

Fig. 12. Picture of the two LISNs equipped with the adapters used to perform the measurement of the scattering parameters.

plane as close as possible to the LISNs inputs. A picture of the test setup is shown in Fig. 12. The scattering parameters matrix resulted from the measurements carried out with the VNA was processed to de embed the impedances introduced by the two adapters using the method proposed in [22], then the elements of $\mathbf{F}$, i.e., the trans-impedances, were evaluated by means of (20), (21), (24) and (25). The magnitude of such parameters vs. frequency is shown in Fig. 13 with different colors. Actually, such parameters were evaluated from the measurements carried out with (red dashed line) and without (blue continuous line) the negative pole of the power supply connected to the reference plane (connection A in Fig. 10) to be able to apply the proposed approach in both cases and to check the influence of the A connection. Based on the plots in Fig. 13, it can be concluded that the connection of the negative power supply to the reference plane changes the trans-impedances at low frequency, i.e., between 100 kHz and 400 kHz, and it is irrelevant above 400 kHz. Such a difference can be ascribed to the low isolation provided by the LISNs at low frequency, as it is also highlighted in Section III-C.

Once completed the characterization of the power supply section, i.e., the two LISNs connected to the dc power supply (a 12 V lead-acid battery), the EUT and its inductive load were included in the test bench and the power supply terminals were connected to the LISNs' EUT ones. The power inverter was operated at 50 kHz and the duty cycle of each PWM signal was regulated to be $\delta = 0.5$. Furthermore, the battery negative terminal was shorted to the reference plane (A connection in Fig. 10), whereas the inverter and the load metal cases were kept isolated from the reference plane.

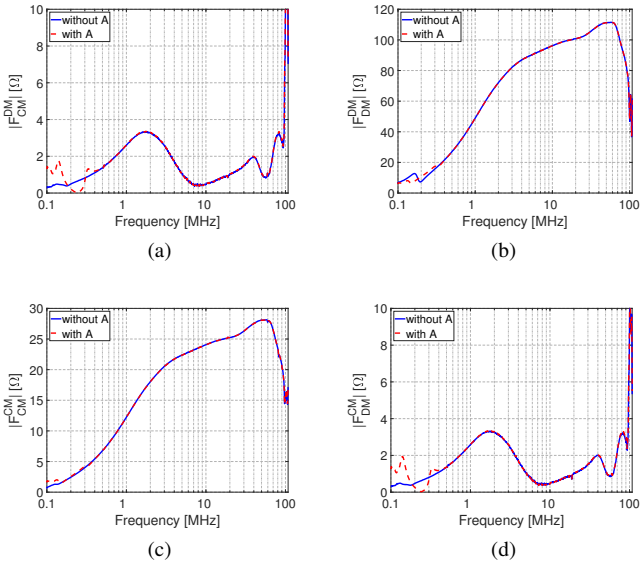

Fig. 13. Transimpedances obtained from the measured scattering parameters. The plots in blue were obtained from the measurements carried out with the negative power supply terminal not connected to the reference plane, i.e., without A, those in red with A.

Aiming to validate the proposed approach, the CM voltage obtained from the measurement at the LISNs outputs was evaluated by (1), then used to calculate the CM current as

$$I_{\mathrm{CM,eq}} = \frac{V_{\mathrm{CM}}^{(m)}}{F_{\mathrm{CM}}^{\mathrm{CM}}} \tag{28}$$

obtaining the spectrum plotted in blue in Fig. 14. Since the LISNs mismatch causes the modal conversion, $I_{\mathrm{CM,eq}}$ is affected by the DM current. In order to prove that, the CM current was measured with the current probe and the EMI receiver included in the test bench shown in Fig. 10 obtaining the spectrum shown in Fig. 14 in yellow. At low frequency, meaning from 150 kHz to 3 MHz, the two spectra differ at the envelopes and harmonic content. Indeed, that obtained from the measurements carried out at the LISNs outputs (blue plot) comprises both even and odd harmonics, whereas that measured with the current probe has odd harmonics only. This difference can be explained observing that the CM loop is driven by the inverter output voltages (nodes U and V in Fig. 11), which are trapezoidal with duty cycle $\delta = 0.5$ and switching frequency $f_{\mathrm{SW}} = 50$ kHz. Therefore, the CM current spectrum should be comprised of odd harmonics only, as it resulted from the direct measurement carried out with the current probe. The even harmonics in it (blue spectrum), which resulted from the measurements at the LISNs' output ports, are likely due to the DM current flowing in the power supply cables, which is converted into CM because of the LISNs mismatch. In the frequency range 3 MHz - 60 MHz the two spectra are almost overlapped. The small difference between them can be ascribed to the calibration of the current probe. Above 60 MHz, the two spectra differ significantly because the current probe was out of its operating bandwidth. Finally, the DM to CM conversion due to the LISNs mismatch was removed from the CM current resulted from the voltages measured at the LISNs output ports using (26). The corrected

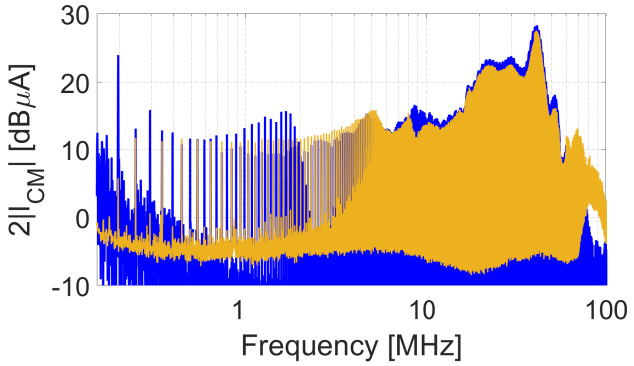

Fig. 14. CM current spectra obtained from the voltages measured with the oscilloscope connected to the LISNs' output ports (blue) and with the EMI receiver connected to the current probe (yellow), respectively.

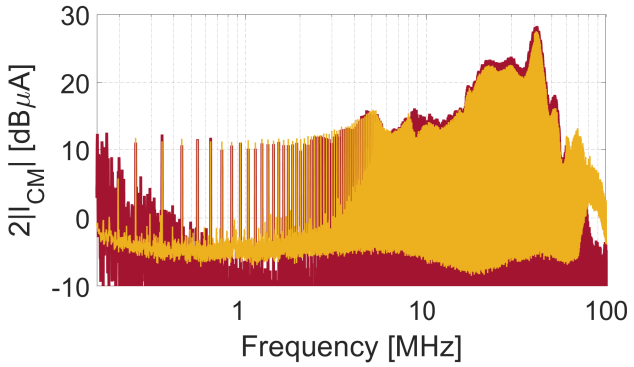

Fig. 15. CM current obtained from the voltages measured at the LISNs output ports with the proposed method (red) and measured with the EMI receiver and the current probe (yellow).

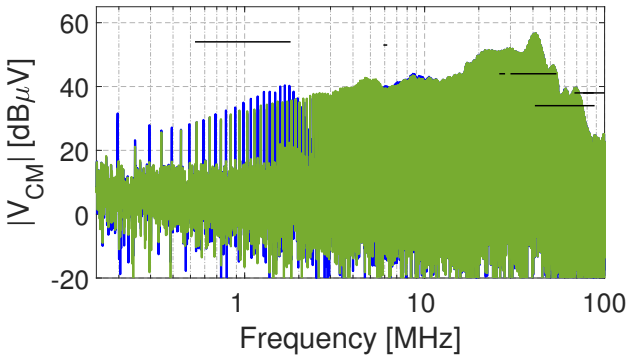

Fig. 16. CM conducted emission spectra obtained from the voltages measured at the LISNs outputs with (green) and without (blue) the correction of the modal conversion proposed in this work. The CISPR 25 emission limit is shown in black.

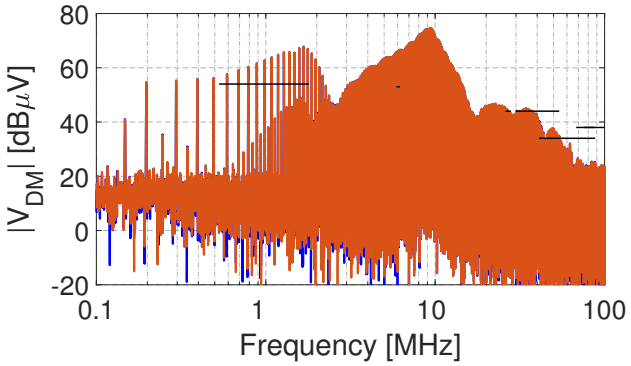

Fig. 17. DM conducted emission spectra obtained from the voltages measured at the LISNs outputs with (orange) and without (blue) the correction of modal conversion proposed in this work. The CISPR 25 emission limit is shown in black.

output spectrum is shown in red in Fig. 15 along with that obtained with that measured with the current probe and the EMI receiver in yellow. It can be noted that, at low frequency, i.e., between 150 kHz and 3 MHz, the red spectrum matches well the yellow one. Moreover, the noise affecting the spectra in Fig. 14 and in Fig. 15, which resulted from the measurement at the LISNs' output ports is due to the FFT of the measured voltages. Finally, (27) was used to evaluate the actual CM and DM conducted emission from those measured at the LISNs output ports. The spectra plotted in green and in orange in Fig. 16 and in Fig. 17 were obtained. These can be compared with those resulted from (1) and (2), which are plotted in blue in the same figures. For the sake of completeness, the CISPR 25 emission limit applicable to out test case is also included (black line).

By these plots, it comes out that the correction of the modal conversion due to the LISNs mismatch is needed for the CM but it is marginal for the DM, since the corrected spectrum in Fig. 17 is almost overlapped to that obtained by (2).

VII. Conclusion

The evaluation of the conducted emission delivered by electronic modules is usually carried out referring to international standards like CISPR 25, which prescribes the use of proper filters, the so called LISNs, to stabilize the power supply impedance over the frequency range of interest, i.e., from 150 kHz to 108 MHz. Such filters allow one to measure the conducted emission delivered by an EUT through its power supply cables, and if the two LISNs test set up is used, to evaluate the CM and the DM components. The analysis and the measurements carried out within this work have highlighted that the traditional methods used to separate such emission components are not effective in the low frequency range due to the LISNs mismatch, which is the main cause of modal conversion. This means that, the CM emission obtained from the LISNs output voltages is affected by the DM one and vice versa. Wanting to address this issue, a method to remove the modal conversion from the voltages measured at the output ports of mismatched LISNs has been developed and validated comparing the CM current delivered by a power inverter, which resulted from the measurement at the LISNs outputs, with that measured by means of a current probe clamped to the power supply cables and connected to an EMI receiver. Finally, the analysis and the measurements showed that the proposed approach is needed especially at low frequency, from 150 kHz to 3 MHz in our case, where the impedance mismatch of two LISNs compliant with the same standard can be greater than that above 10 MHz, which is dominated by the termination

resistance value.

REFERENCES

[1] CISPR 25 - "Vehicles, boats and internal combustion engines - Radio disturbance characteristics - Limits and methods of measurement for the protection of on-board receivers" - 2016 - IEC.

[2] CISPR 14 - "Electromagnetic compatibility - Requirements for household appliances, electric tools and similar apparatus"; 2016; IEC.

[3] CISPR 16 - "Specification for radio disturbance and immunity measuring apparatus and methods"; 2015; IEC.

[4] H.W. Ott, "Electromagnetic Compatibility Engineering", Wiley, 2009.

[5] H. Zhang and S. Wang, "EMI noise source modeling based on network theory for power converters with mixed-mode characterization" *Proc. of 2018 IEEE Applied Power Electronics Conf. and Exp. (APEC)*, 2018, pp. 984-991.

[6] M.J. Nave, "A Novel Differential Mode Rejection Network for Conducted Emissions Diagnostics", *IEEE Nat. Symp. on Electromagnetic Compatibility*, May 1989.

[7] S. Wang, F.C. Lee, W.G. Odendaal, "Characterization, Evaluation and Design of a Noise Separator for Conducted EMI Noise Diagnosis" *IEEE Trans. on Power Electronics*, vol. 20, n. 4, Jul. 2005.

[8] L. Zhang, K. Wang, J. Meng, W.M. Ma, "The Fabrication and Application of CM/DM Interference Separation Network Based on Transmission-line Transformer" *Proc. Asia-Pacific Int. Sym. on EMC*, Apr. 2010.

[9] C.R. Paul, K.B. Hardin, "Diagnosis and Reduction of Conducted Noise Emissions" *IEEE Trans. on Electromagnetic Compatibility*, vol. 30, n. 4, Nov. 1988.

[10] A. A. Ramesh, B. Subbarao, R. Sivaramakrishnan, "Design of low cost common and differential mode noise diagnostic circuit" *Proc. of the 9th Int. Conf. on EM Interf. and Comp. (INCEMIC)*, Feb. 2006.

[11] T. Cui, Q. Ma, P. Xu, "A New Method of Eliminating Indeterminacy in ICA for Conducted EMI Separation" *Proc. IEEE Int. Pow. Electr. and Motion Control Conf.*, May 2016.

[12] J. Stahl, D. Kuebrich, A. Bucher, T. Duerbaum, "Characterization of a Modified LISN for Effective Separated Measurements of Common Mode and Differential Mode EMI Noise" *Proc. IEEE Energy Conv. Congr. and Exp. (ECCE)*, Sept. 2010.

[13] J. Cho et al., "Mixed-Mode ABCD Parameters: Theory and Application to Signal Integrity Analysis of PCB-Level Differential Interconnects", *IEEE Transactions on Electromagnetic Compatibility*, vol. 53, no. 3, pp. 814-822, Aug. 2011

[14] W. Fan, A. Lu, L.L. Wai and B.K. Lok, "Mixed-mode S-parameter characterization of differential structures", *Proc. of the 5th Electr. Packaging Tech. Conf. (EPTC 2003)*, Singapore, 2003, pp. 533-537.

[15] P. S. Crovetti and F. Fiori, "Distributed Conversion of Common-Mode Into Differential-Mode Interference", *IEEE Transactions on Microwave Theory and Techniques*, vol. 59, no. 8, pp. 2140-2150, Aug. 2011.

[16] S. Negri, X. Wu, X. Liu, F. Grassi, G. Spadacini and S.A. Pignari, "Mode Conversion in DC-DC Converters with Unbalanced Busbars", *2019 Joint Int. Sym. on Electromagnetic Comp., Sapporo and Asia-Pacific Int. Sym. on Electromagnetic Comp.*, Sapporo, 2019, pp. 112-115.

[17] S. Wang and F. C. Lee, "Investigation of the Transformation Between Differential-Mode and Common-Mode Noises in an EMI Filter Due to Unbalance", *IEEE Transactions on Electromagnetic Compatibility*, vol. 52, no. 3, pp. 578-587, Aug. 2010.

[18] H.R. Ahn, "Asymmetric Passive Components in Microwave Integrated Circuits", *Appendix B*, Wiley, 2006.

[19] M.M. Jha, K.B. Naik, S.P. Das, "Analysis of Dominant Frequency Ranges for Various Modes of EMI Generated by Switching Converters" *Proc. Joint Int. Conf. on Pow. Electr., Drives and Ener. Sys. (PEDES)*, Dec. 2010.

[20] M. Perotti and F. Fiori, "Investigating the EMI Mitigation in Power Inverters Using Delay Compensation", *IEEE Tran. on Power Electronics*, vol. 34, no. 5, pp. 4270-4278, May 2019.

[21] Keysight, *E5080A*, https://www.keysight.com/en/pdx-x202208-pn-E5080A

[22] K. Steinberg, M. Scheffler, and M. Dressel, "Microwave inductance of thin metal strips", *Journal of Applied Physics*, vol. 108, n.9, 2010.

[23] Messtec, *AN20200*.

[24] Tektronix, *P6021* Current probe User Manual, https://download.tek.com/manual/070094706.pdf

[25] Rhode&Schwarz, *ESRP* EMI Receiver User Manual, https://www.rohde-schwarz.com

[26] Teledyne Lecroy, *HDO9404* Digital Oscilloscope User Manual, http://cdn.teledynelecroy.com/files/pdf/hdo9000-oscilloscope-datasheet.pdf